Effect of plastic coating on the density of plasma formed in Si foil targets irradiated by ultra-high-contrast relativistic laser pulses

A. S. Martynenko [1,2] S. A. Pikuz [1,2,*] I. Yu. Skobelev [1,2] S. N. Ryazantsev [1,2] C. Baird [3] N. Booth [4]
L. Doehl [3] P. Durey,[3] A. Ya. Faenov [1,5] D. Farley [3] R. Kodama,[5,6] K. Lancaster,[3] P. McKenna [7] C. D. Murphy,[3]
C. Spindloe,[4] T. A. Pikuz,[1,5] and N. Woolsey [3]

[1]*Joint Institute for High Temperatures of Russian Academy of Sciences, 125412 Moscow, Russia*
[2]*National Research Nuclear University MEPhI, Kashirskoe Sh. 31, 115409 Moscow, Russia*
[3]*York Plasma Institute, Department of Physics, University of York, York YO10 5DD, England, United Kingdom*
[4]*Central Laser Facility, STFC Rutherford Appleton Laboratory, Didcot OX11 0QX, England, United Kingdom*
[5]*Open and Transdisciplinary Research Initiative, Osaka University, Osaka 565-0871, Japan*
[6]*Institute of Laser Engineering, Osaka University, Suita 565-0871, Japan*
[7]*Department of Physics, SUPA, University of Strathclyde, Glasgow G4 0NG, Scotland, United Kingdom*

The formation of high energy density matter occurs in inertial confinement fusion, astrophysical, and geophysical systems. In this context, it is important to couple as much energy as possible into a target while maintaining high density. A recent experimental campaign, using buried layer (or "sandwich" type) targets and the ultrahigh laser contrast Vulcan petawatt laser facility, resulted in 500 Mbar pressures in solid density plasmas (which corresponds to about 4.6×10^7 J/cm^3 energy density). The densities and temperatures of the generated plasma were measured based on the analysis of x-ray spectral line profiles and relative intensities.

I. INTRODUCTION

Studies of high energy density matter (>1 Mbar, 100 GPa, 10^{11} J/m^3) have been of great interest for various fields of science, such as astrophysics, physics of plasma, thermonuclear fusion, and particle acceleration technologies [1]. Different methods based on the compression and heating of matter by shock waves (for example, generated by gas guns, pinch discharges, or high-power lasers) are commonly used to create such states under laboratory conditions. If a material is heated almost instantaneously, for example, by using a sufficiently short duration heating source, then the compression stage might be unnecessary. Using this isochoric approach, it is relatively easy to achieve high energy density conditions using short-pulse lasers at relativistic intensities [2–6].

It is of fundamental importance to know the plasma conditions as laser energy is deposited into a target and this is particularly challenging when a laser pulse has a sufficiently intense prepulse. In the case of a laser with a poor contrast ratio, the prepulse forms an extended region of plasma with densities below the critical density [7]. This means that isochoric formation of high energy density matter close to solid density is not possible where the contrast ratio (i.e., the ratio of the laser peak intensity to the intensity of the pulse pedestal) exceeds 10^{12} [6]. Furthermore, laser technology improvements (resulting in intensities exceeding 10^{23} W/cm^2) will require ever higher laser contrast.

The characteristic time between the front of the intense laser pedestal and the main laser pulse is about 10 ps [17]. Taking preplasma expansion speed to be $v_{\exp} \sim 10^6 - 10^7$ cm/s (which is of the order of the speed of sound), and the skin layer thickness $l_0 \sim 0.1 \, \mu$m (for a laser wavelength of $1 \, \mu$m), one can estimate that the preplasma volume increases by about a factor of 2–10 before the main laser pulse arrival. In other words, the main energy of the heating laser pulse is deposited in a target with a density which is significantly lower than the solid-state one because of the intense laser pedestal. Coating is supposed to significantly increase the lifetime of the solid-state preplasma. A transparent coating layer deposited on the front or on both target surfaces may prevent the expansion of the preplasma keeping the target density close to the solid-state one, at least at picosecond time scale.

In general, the formation of preplasma is not problematic unless the preplasma expansion significantly affects the target of interest. One solution is to delay the impact of preplasma expansion by sandwiching the material of interest in a multilayered target, known as tamping.

The implementation of target coating and tampering in laser-matter interaction experiments has a substantial background. Plastic absorbing coatings have been used as a compressor for spherical thermonuclear targets in inertial confinement studies since the early 1970s [8,9]. At the same time, experiments on the laser irradiation of coated (layered) solid targets began [10–12]. Much later, it was proposed to use laser transparent target coatings to prevent a preplasma formation by a prepulse of a powerful pico- or femtosecond laser pulse [13–16].
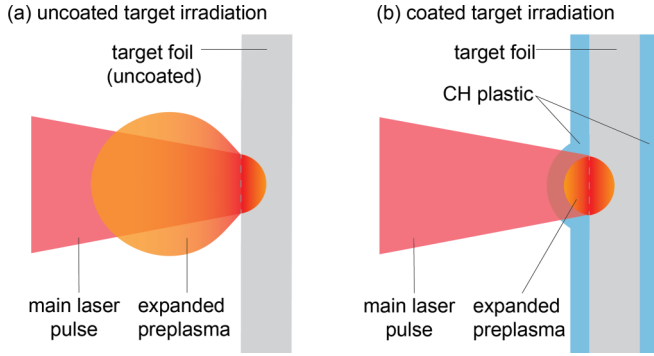
*spikuz@gmail.com

FIG. 1. Schematic comparison of an intense laser pulse interacting with a solid density target and the formation of preplasma on the target surface in case of a (a) plain foil target and (b) sandwich type target (a preplasma forms at the inner interface between the outer and inner layer in a sandwich target).

FIG. 2. Experimental schematic showing the relative positions of the target foil, laser pulse, plasma mirror, and the three FSSR spectrometers.

The outer layer of the target is usually formed from material with a higher ionization threshold than the inner material and is also transparent to laser radiation. As the laser prepulse intensity increases, any preplasma at the interface between the outer and inner layers, as is illustrated in Fig. 1(b), is confined by the inertia of the outer layer. This impedes the expansion of the plasma of interest, helping to maintain a high density ideally until the arrival of the main pulse. The use of a sandwich targets demands a high laser contrast, yet in general the requirements for the laser contrast are noticeably lower.

Contrast measurements of high-contrast lasers are difficult to make, and it is almost impossible to *a priori* predict the laser contrast for each laser shot. Here we use x-ray spectroscopy to study high-contrast laser interactions with sandwich targets up to laser intensities of 6×10^{20} W/cm^2. We compare emission from plain foil targets and sandwich targets, and find that the use of sandwich targets allows the material to remain close to a solid density with an energy density of about 5×10^7 J/cm^3 or 500 Mbar.

II. EXPERIMENTAL DATA

The experiment was conducted on the Vulcan Nd: glass (with a wavelength of 1054 nm) petawatt laser system at the Rutherford-Appleton laboratory (UK) [17]. For each shot, the *p*-polarized laser beam delivered ~300 J on the target in a ~1 ps pulse and was focused onto a target using an f/3 off-axis parabola. This produced a focal spot containing approximately 30% of the energy in a 7 μm diameter region. Using Optical Parametric Chirped-pulse Amplification (OPCPA) [1] and a plasma mirror [18–20] placed just before the focal plane, the laser contrast exceeded 10^{10} at 1 ns [21]. See the top view of the experimental setup in Fig. 2. The angle of incidence of laser to the target surface was 45°. We compare the x-ray emission from plain and CH plastic-coated μm-thick solid Si foils using three focusing spectrometers with spatial resolution (FSSR) [22,23]. The spectrometers recorded emission at ~5° to the target surface normal (see Fig. 2) with spherically bent quartz crystals and image plate detectors. These spectrometers were designed to record spectral emission at high 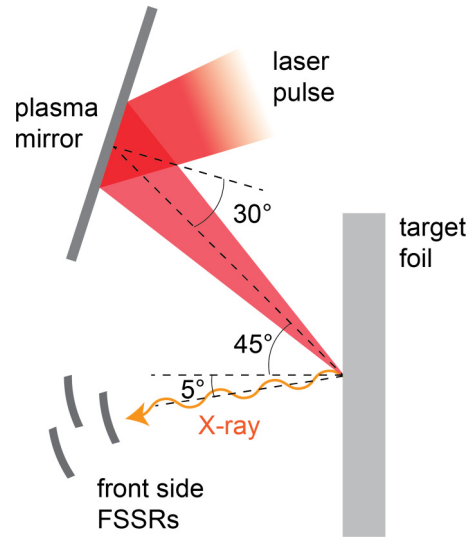resolution across different parts of the spectrum and to cover a continuous yet broad spectral range that extends from 4.5 to 7.5 Å as summarized in Table I.

Overlapping the spectral ranges of each spectrometer enables cross-calibration of spectral intensities as well as the facility to accurately identify and subtract bremsstrahlung contribution in the measurement. A more detailed description of the experiment is contained in Ref. [18].

The four spectra in Fig. 3 are from (i) a low-contrast laser interaction with a 0.5 μm thick SiN target and (ii–iv) high-contrast interactions with 0.5 μm thick SiN, 2 μm thick Si, and 2 μm thick Si targets coated with 1.4 μm thick CH plastic, respectively. Data extraction for all spectra uses the same methodology. The spectra are space and time integrated and the emission is dominated by the densest and hottest region of the plasma. The low-contrast measurement, spectrum (i), used a standard mirror in place of the plasma mirror. This mirror reflects most of the laser prepulse and the target foil expands. As a result, the main part of the laser pulse heats an extended low-density plasma. There is a clear signature of this in the emission spectrum which is characterized by relatively narrow and well distinguished lines from silicon H- and He-like ions and associated satellites. Further analysis shows that the spectral linewidths are consistent with a near critical density plasma. The narrow spectral lines allow the use of this spectrum to verify and accurately set the dispersion of the three spectrometers and then as a reference enabling the precise determination of the spectral line positions in all spectra. The spectral line centers of the Si XIV (Si^{13+}) Ly$_\alpha$, Ly$_\beta$ lines and Si XIII (Si^{12+}) He$_\alpha$, He$_\beta$ are shown by the

TABLE I. Spectral ranges of each FSSR described in experiment.

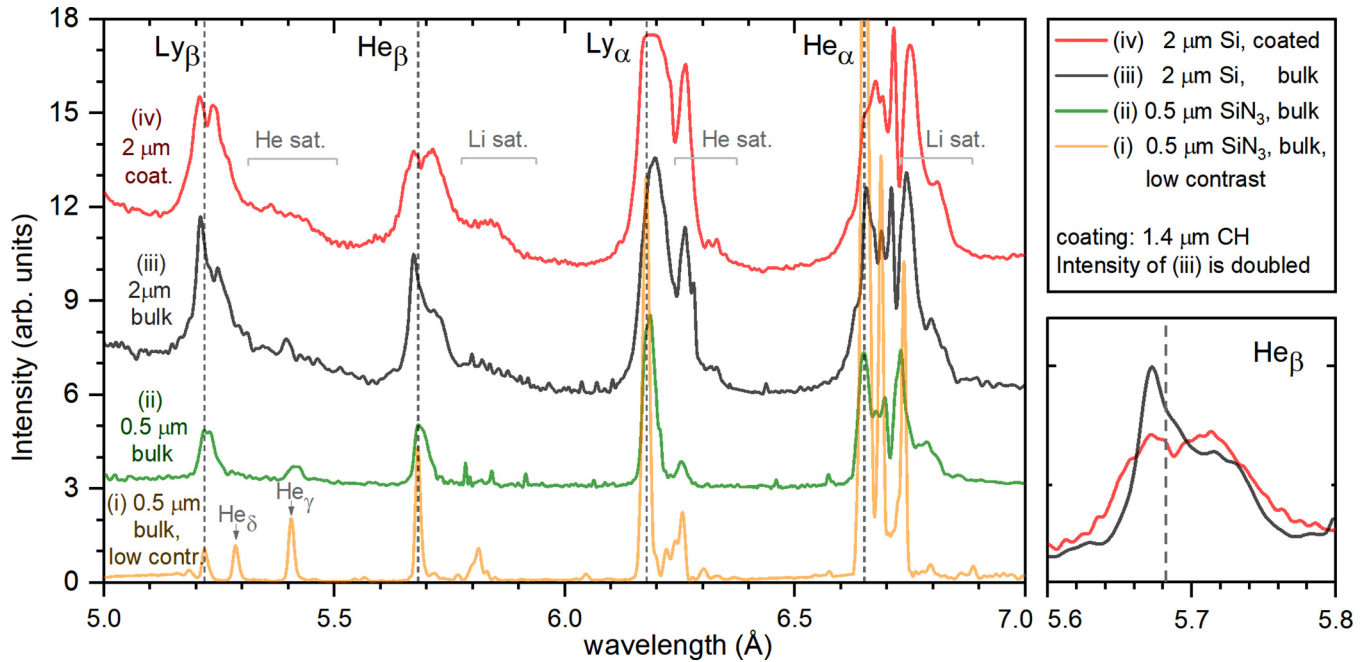| Spectrometer number	1	2	3
Spectral range (Å)	4.5–5.8	5.5–6.9	6.6–7.5

FIG. 3. Experimental x-ray spectra obtained by laser pulse irradiation of a (i) 0.5 μm SiN$_3$ uncoated foil (orange curve) without plasma mirror, (ii) 0.5 μm SiN$_3$ uncoated foil (green curve) with plasma mirror, (iii) 2 μm Si foil coated on both sides with 1.4 μm CH plastic layers (red curve), and (iv) 2 μm Si uncoated foil (black curve). For ease of comparison, the intensity of the curve (i) was divided by factor 2 and the intensity of the curve (iii) was increased by factor 2.

vertical dashed lines. In addition, the He$_\gamma$ and He$_\delta$ resonance lines are clearly resolved in spectrum (i).

In spectrum (ii) the high contrast laser interacts with a 0.5 μm SiN$_3$ foil and the spectral lines are much broader than in spectrum (i). The spectral resonance lines appear to broaden to the long wavelength side of the resonance line centres. This broadening is characteristic of a higher density plasma and results from a combination of increased Stark broadening and increasing recombination rate that populates the satellite states. Dense plasma effects result in similar line intensities in the Ly-like and He-like series and disappearance of the He$_\delta$ line. The spectral lines remain clearly resolved and this indicates that the plasma density is higher than critical density but lower than solid.

Increasing the thickness of a target results in more hot material remaining at near solid density during the laser interaction, and as a result emission may be dominated by a plasma of higher density. Spectrum (iii) is from a 2 μm thick Si foil and shows strong emission from Ly$_\alpha$, Ly$_\beta$ and He$_\alpha$, He$_\beta$ lines. These lines are broader than spectral lines observed in spectrum (ii), and satellite structure on the long wavelength side of these lines is more prominent with this structure extending towards the adjacent resonance line. As a result, the spectral lines are not as well resolved. For example, the He$_\beta$ transition line is partially overlapped with He-like satellites to the Ly$_\beta$ transition line in a region of 5.5–5.7 Å. The asymmetry of the spectral line profiles close to the line centers (indicated by the vertical dashed line) is indicative of self-absorption in the plasma. For example, the optical mean free path of Ly$_\beta$ radiation is comparable to the 2 μm thickness of the target, i.e., an optical depth of approximately 1.

The fourth spectrum (iv) is from 2 μm Si foil with a 1.4 μm outer layer of CH plastic on both front and rear sides.

Here the spectral lines are broad and overlapping, with rather symmetrical Ly$_\beta$ and He$_\beta$ line profiles; in comparison the Ly$_\alpha$ and He$_\alpha$ are optically thick and strongly modified by opacity effects. The central dip close to the line center of the Ly$_\beta$ and He$_\beta$ transitions is caused by the self-absorption. A comparison of the integrated spectral intensity in these spectral lines across spectra (ii), (iii), and (iv) shows the emission is greatest from the sandwich target. This results from the inertial tamping of the target by the plastic layer and increased density.

There is a noticeable shift of Ly$_\beta$, He$_\beta$ line positions in spectra (ii), (iii), and (iv) compared to spectra (i); this is likely due to the compression of electron energy levels and a decrease in the energy of the photons emitted in a dense plasma, which was discussed in Ref. [24]. The consistency of the effect was confirmed by the examination of several targets with slightly different coatings and thicknesses of the main foil.

III. NUMERICAL SIMULATION AND DATA ANALYSIS

Quantitative assessment of plasma parameters relies upon atomic and plasma synthesis models; here we compare measurement with the radiation-collisional kinetic code PRISM-SPECT [25,26].

As discussed above, a preliminary analysis suggests near-solid plasma density in cases (iii) and (iv). The conditions of near-solid density and high temperature occur shortly after the arrival of the main laser pulse; this results in the most significant contribution to the total spectrum. Here, the modeling of the emission spectrum uses a stationary approximation; we demonstrate this is sufficient to describe the experimental data below. In comparison, in case (i) a prepulse (as the laser
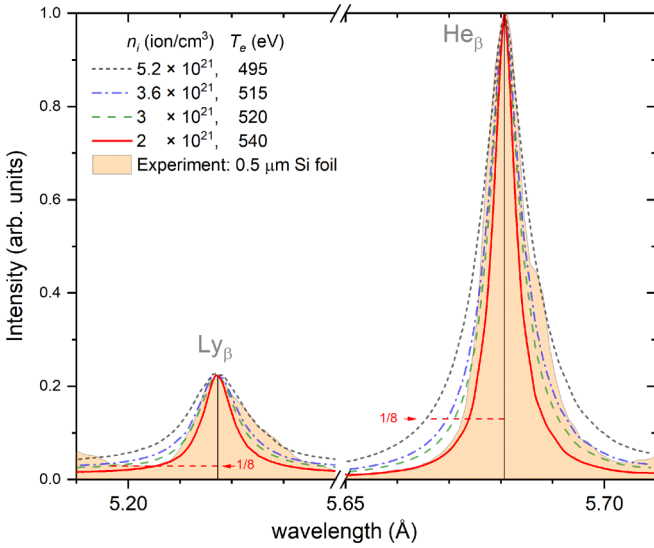
FIG. 4. Comparison of numerically calculated and experimental spectra (an orange area) for Ly_β and He_β lines emitted by the 0.5 μm SiN_3 foil during irradiation by a high contrast laser beam (plasma mirror was not used). The spectra are modeled for different initial plasma parameters (color curves) in the approximation of plasma adiabatic expansion approach (initial plasma parameters are presented in the legend); solid line represents the best fit.

is used without a plasma mirror) forms a preplasma from the uncoated target. This preplasma expands significantly before the arrival of the main laser pulse. This leads to absorption of the intense laser pulse energy in a plasma of noticeably lower density. We find the analysis of case (i) must include the plasma expansion as well as late stages in the

plasma evolution to simulate the spatially and time-integrated spectrum.

A. Thin uncoated target

A numerical simulation of Ly_β and He_β spectral lines was performed according to an adiabatic expansion approach developed in Ref. [27]. Comparison of the calculated spectra with the experimental one was performed as shown in Fig. 4.

The Ly_β and He_β spectral lines have low opacity with widths that are sensitive to variations of plasma parameters and line broadening is most easily seen in the wings of the profile, where the emission from initial stages of plasma expansion makes the major contribution. Thus, it is more advantageous to compare the model and experimental line profiles at the lowest possible relative intensities, to ensure accurate evaluation of plasma density evaluation during the initial stages of the expansion. This is possible at the 1/8 level of the spectral line maxima due to the low level of the noise in the experiment. There is clear asymmetry of the spectral line profile with the red wing broadened by satellite transitions. Resonant line (Ly_β and He_β) profile analysis uses the blue (short-wavelength) wing of each line. This approach gives an ion and electron density of $2(\pm 0.5) \times 10^{21}$ ion/cm^3 and $2.5(\pm 0.5) \times 10^{22}$ electron/cm^3, respectively, and temperature of about 520 eV; this is shown as the red solid curve in Fig. 4 with an average energy density in a range of $2(\pm 0.5) \times 10^6$ J/cm^3. The estimated plasma density is more than one order of magnitude lower than solid density. At these densities, the emission lines will have negligible line center shifts; the spectrum from case (i) is used as a reference spectrum. The dot-dashed curves in Fig. 4 illustrate the data quality and the precision of the line-shape comparisons.
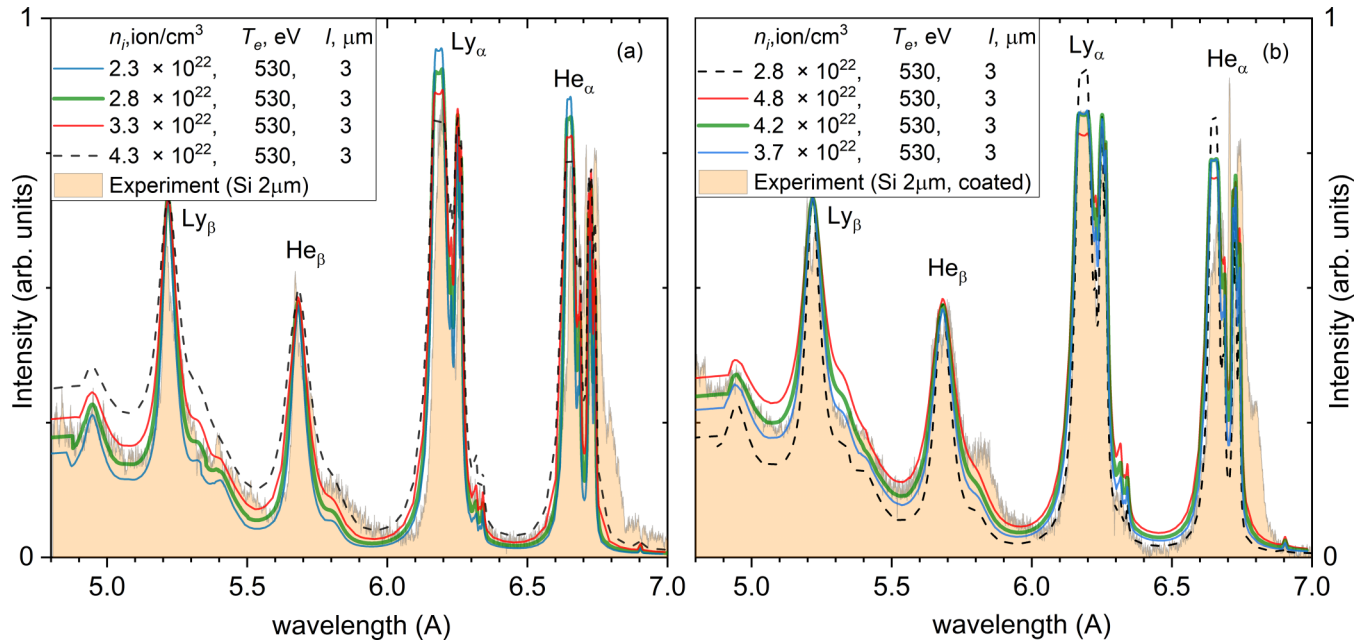

FIG. 5. Simulation data calculated in the stationary approximation (colored lines) in comparison with experimental spectra (orange regions) for (a) an uncoated 2 μm Si foil, case (iii), and (b) 1.4 μm CH + 2 μm Si + 1.4 μm CH, case (iv). Solid green lines are best fits; red and blue curves are over- and underestimations, respectively. The ion density, electron temperature, and plasma thickness denoted by n_i, T_e, and l, respectively, are given in the legend.

B. Thick coated and uncoated targets

High near solid density is expected in cases (iii) and (iv), which use a very high-contrast laser pulse and thick and buried targets, respectively. Using a homogeneous and stationary approximation (i.e., time constant single density and temperature). It is possible to find a good match between the model and experimental spectra. This is clearly demonstrated across a wide spectral range (4.8–7 Å) for the thick bulk target case (iii) in Fig. 5(a) and for the buried layer case (iv) in Fig. 5(b). To determine the range of suitable plasma parameters, the plasma density, temperature, and optical thickness of the plasma were varied in the spectra modeling with respect to the best-fit case until the deviation between modeled and experimental spectra becomes significant. In the comparison, to estimate plasma density and thickness we considered Ly_α/Ly_β and He_β/Ly_β line intensity ratios, and widths of Ly_β and He_β lines as illustrated in Fig. 6 for a 2 μm silicon coated target. Of all the mentioned cases, only the He_β/Ly_β ratio shows a significant temperature dependence as shown in Fig. 6(c). The given model curves were obtained for fixed plasma thicknesses of 2 and 3 μm, but other values were considered as well. Filled areas represent the ranges of ion density derived from particular spectra parameters observed. As seen, for the plasma thickness of 2 μm [Fig. 6(a)] there is no plasma density satisfying both line intensity ratios, while for 3 μm thickness [Fig. 6(b)] the density range of $4.2(\pm0.5) \times 10^{22}$ ion/cm^3 was certainly found. Dashed lines in Fig. 5 show how the data quality enables accurate determination of the plasma density. There are differences between the modeled and experiment line shapes. These differences are mainly due to He-like satellites of Ly_α and Ly_β as well as Li-like satellites of He_α and He_β transition lines. Emission from these satellites is stronger at lower temperature, suggesting this spectral component comes from material at a lower temperature. We suggest these satellites originate from material in the regions around the laser spot and from late stages of the experiment after the main laser and as the plasma expands and cools. Peripheral or late stage plasma was relatively cold or less dense, so it was sufficiently less contributing to the integrated experimental spectra [27]. It causes some underestimation of plasma density and temperature. Therefore, ranges of 5.4–5.6, 5.75–6, and 6.75–7 Å of experimental spectra are not well described in the modeling.

Our comparison of the resonance line transitions in the model and experimental spectra suggests peak ion and electron densities, and temperature, of $2.8(\pm0.5) \times 10^{22}$ ion/cm^3, $3.6(\pm0.6) \times 10^{23}$ electron/cm^3, and 520–540 eV, respectively, and a plasma thickness of 3–3.3 μm for spectrum (iii). The nominal target thickness was 2 μm of uncoated Si. The average energy density for this plasma parameters is $3.1(\pm0.5) \times 10^7$ J/cm^3.

The spectrum (iii) shows spectral line shifts, which are probably dense plasma effects not included in the PRISMSPECT code, therefore they were accounted for by a manual shifting of wavelengths of Ly_β, He_β lines of calculated spectra using the approach implemented in Ref. [24]. The He_β/Ly_β ratio shows strong dependence on plasma density [27].

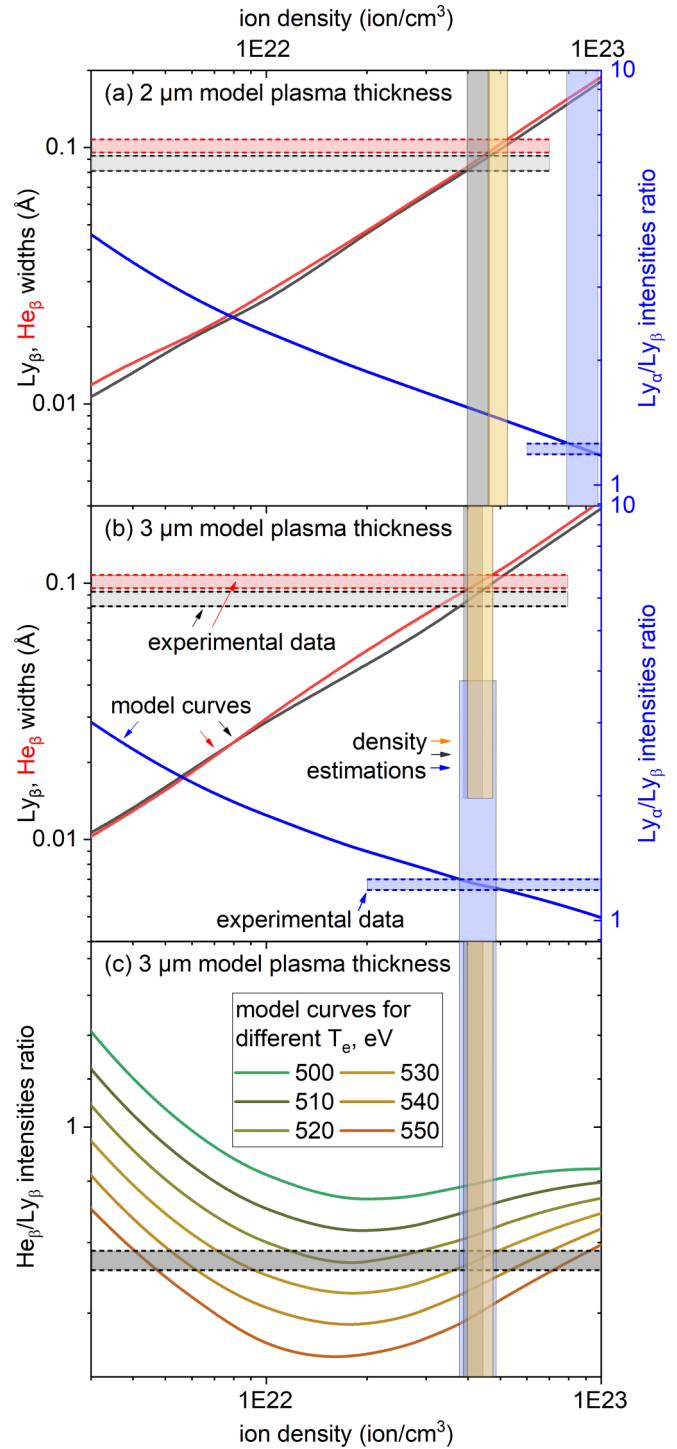Model comparison with the experimental spectrum (iv) suggests ion and electron densities of $4.2(\pm0.5) \times$

FIG. 6. The dependence of Lya, Heb linewidths, and Ly_α to Ly_β intensity ratio on plasma density as calculated for (a) 2 um and (b) 3 um optically thick Si plasma and (c) Heb to Lyb intensity ratio for a set of electron temperatures depending on plasma density. The range of values obtained in experiment with a 2 um Si CH-coated target and corresponding plasma densities are shown by filled bars.

10^{22} ion/cm^3 and $5.4(\pm0.6) \times 10^{23}$ electron/cm^3, respectively. The temperature and thickness are 520–540 eV and 2.8–3.1 μm, respectively. This gives an average energy density of $4.6(\pm0.5) \times 10^7$ J/cm^3. The inferred plasma densities

for cases (iii) and (iv) are close to the solid-state density. This indicates that there was no significant preplasma or target expansion prior to the interaction with the main laser pulse. Furthermore, the plasma density of the plastic-coated target, case (iv), is higher than the uncoated target, case (iii). Therefore, the use of a plastic layer increases the plasma confinement.

IV. CONCLUSION

In this paper, we experimentally studied time-integrated x-ray emission spectra of 2 and 0.5 μm Si foils irradiated with ultra-high-contrast relativistic intensity laser beams of the Vulcan petawatt facility (UK). We compared spectra for coated (with CH plastic) and uncoated targets, for high and ultrahigh laser contrast cases. An analysis of relative heights and profiles of spectral lines and comparison with numerical spectra of a radiation-collisional kinetic code allow us to distinguish plasma with quite close parameters. Based on that, it was confirmed that irradiation of a few-μm-thick bulk solid target with the ultra-high-contrast laser can generate a hot plasma only a factor of 2 or 3 lower than solid density. We find that only the use of targets buried in μm-thick plastic layers can ensure even higher densities, up to near solid, which is of great interest in high energy density experiments. Correspondingly, silicon dense plasma states were obtained with an energy density of about 4.6×10^7 J/cm^3 and ion density of $4.2(\pm 0.5) \times 10^{22}$ ion/cm^3, which is 0.8–0.9 of the solid density.

Thus, in this paper, we proposed and tested the approach based on the x-ray emission spectral diagnostic that allows us to estimate the plasma density of coated targets. The use of sandwich type targets allows us to ensure the conditions of isochoric heating.

[1] G. A. Mourou, T. Tajima, and S. V. Bulanov, Rev. Mod. Phys. **78**, 309 (2006).

[2] J. H. Sung, H. W. Lee, J. Y. Yoo, J. W. Yoon, C. W. Lee, J. M. Yang, Y. J. Son, Y. H. Jang, S. K. Lee, and C. H. Nam, Opt. Lett. **42**, 2058 (2017).

[3] S. Gales, K. A. Tanaka, D. L. Balabanski, F. Negoita, D. Stutman, O. Tesileanu, C. A. Ur, D. Ursescu, I. Andrei, S. Ataman, M. O. Cernaianu, L. D'Alessi, I. Dancus, B. Diaconescu, N. Djourelov, D. Filipescu, P. Ghenuche, D. G. Ghita, C. Matei, K. Seto, M. Zeng, and N. V Zamfir, Reports Prog. Phys. **81**, 094301 (2018).

[4] D. N. Papadopoulos, P. Ramirez, K. Genevrier, L. Ranc, N. Lebas, A. Pellegrina, C. Le Blanc, P. Monot, L. Martin, J. P. Zou, F. Mathieu, P. Audebert, P. Georges, and F. Druon, Opt. Lett. **42**, 3530 (2017).

[5] L. Yu, Y. Xu, Y. Liu, Y. Li, S. Li, Z. Liu, W. Li, F. Wu, X. Yang, Y. Yang, C. Wang, X. Lu, Y. Leng, R. Li, and Z. Xu, Opt. Express **26**, 2625 (2018).

[6] H. Kiriyama, A. S. Pirozhkov, M. Nishiuchi, Y. Fukuda, K. Ogura, A. Sagisaka, Y. Miyasaka, M. Mori, H. Sakaki, N. P. Dover, K. Kondo, J. K. Koga, T. Z. Esirkepov, M. Kando, and K. Kondo, Opt. Lett. **43**, 2595 (2018).

[7] M. A. Alkhimova, A. Y. Faenov, I. Y. Skobelev, T. A. Pikuz, M. Nishiuchi, H. Sakaki, A. S. Pirozhkov, A. Sagisaka, N. P. Dover, K. Kondo, K. Ogura, Y. Fukuda, H. Kiriyama, K. Nishitani, T. Miyahara, Y. Watanabe, S. A. Pikuz, M. Kando, R. Kodama, and K. Kondo, Opt. Express **25**, 29501 (2017).

[8] J. Nuckolls, L. Wood, A. Thiessen, and G. Zimmerman, Nature (London) **239**, 139 (1972).

[9] R. Betti and O. A. Hurricane, Nat. Phys. **12**, 435 (2016).

[10] W. Seka, J.-L. Schwob, and C. Breton, J. Appl. Phys. **42**, 315 (1971).

[11] F. C. Young, R. R. Whitlock, R. Decoste, B. H. Ripin, D. J. Nagel, J. A. Stamper, J. M. McMahon, and S. E. Bodner, Appl. Phys. Lett. **30**, 45 (1977).

[12] B. Yaakobi and T. C. Bristow, Phys. Rev. Lett. **38**, 350 (1977).

[13] D. Riley, J. J. Angulo-Gareta, F. Y. Khattak, M. J. Lamb, P. S. Foster, E. J. Divall, C. J. Hooker, A. J. Langley, R. J. Clarke, and D. Neely, Phys. Rev. E **71**, 016406 (2005).

[14] K. B. Wharton, C. D. Boley, A. M. Komashko, A. M. Rubenchik, J. Zweiback, J. Crane, G. Hays, T. E. Cowan, and T. Ditmire, Phys. Rev. E **64**, 025401(R) (2001).

[15] A. L. Kritcher, P. Neumayer, M. K. Urry, H. Robey, C. Niemann, O. L. Landen, E. Morse, and S. H. Glenzer, High Energy Density Phys. **3**, 156 (2007).

[16] S. N. Chen, G. Gregori, P. K. Patel, H.-K. Chung, R. G. Evans, R. R. Freeman, E. Garcia Saiz, S. H. Glenzer, S. B. Hansen, F. Y. Khattak, J. A. King, A. J. Mackinnon, M. M. Notley, J. R. Pasley, D. Riley, R. B. Stephens, R. L. Weber, S. C. Wilks, and F. N. Beg, Phys. Plasmas **14**, 102701 (2007).

[17] C. N. Danson, P. A. Brummitt, R. J. Clarke, J. L. Collier, B. Fell, A. J. Frackiewicz, S. Hancock, S. Hawkes, C. Hernandez-Gomez, P. Holligan, M. H. R. Hutchinson, A. Kidd, W. J. Lester, I. O. Musgrave, D. Neely, D. R. Neville, P. A. Norreys, D. A. Pepler, C. J. Reason, W. Shaikh, T. B. Winstone, R. W. W. Wyatt, and B. E. Wyborn, Nucl. Fusion **44**, S239 (2004).

[18] I. Y. Skobelev, S. N. Ryazantsev, D. D. Arich, P. S. Bratchenko, A. Y. Faenov, T. A. Pikuz, P. Durey, L. Doehl, D. Farley, C. D. Baird, K. L. Lancaster, C. D. Murphy, N. Booth, C. Spindloe, P. McKenna, S. B. Hansen, J. Colgan, R. Kodama, N. Woolsey, and S. A. Pikuz, Photonics Res. **6**, 234 (2018).

[19] G. Doumy, F. Quéré, O. Gobert, M. Perdrix, P. Martin, P. Audebert, J. C. Gauthier, J.-P. Geindre, and T. Wittmann, Phys. Rev. E **69**, 026402 (2004).

[20] R. Hörlein, B. Dromey, D. Adams, Y. Nomura, S. Kar, K. Markey, P. Foster, D. Neely, F. Krausz, G. D. Tsakiris, and M. Zepf, New J. Phys. **10**, 083002 (2008).

[21] C. Hernandez-Gomez, Central Laser Facility Annual Report 2016- 2017, Rutherford Appleton Laboratory, 2017, pp. 6–8.

[22] A. Y. Faenov, S. A. Pikuz, A. I. Erko, B. A. Bryunetkin, V. M. Dyakin, G. V Ivanenkov, A. R. Mingaleev, T. A. Pikuz, V. M. Romanova, and T. A. Shelkovenko, Phys. Scr. **50**, 333 (1994).

[23] M. A. Alkhimova, I. Y. Skobelev, A. Y. Faenov, D. A. Arich, T. A. Pikuz, and S. A. Pikuz, Quantum Electron. **48**, 749 (2018).

[24] C. R. Stillman, P. M. Nilson, S. T. Ivancic, I. E. Golovkin, C. Mileham, I. A. Begishev, and D. H. Froula, Phys. Rev. E **95**, 063204 (2017).

[25] J. J. MacFarlane, I. E. Golovkin, P. R. Woodruff, D. R. Welch, B. V Oliver, T. A. Mehlhorn, and R. B. Campbell, in *Inertial Fusion Sciences and Applications 2003*, edited by B. A. Hammel, D. D. Meyerhofer, J. Meyer-ter-Vehn, and H. Azechi (American Nuclear Society, La Grange Park, IL, 2004), pp. 457–460.

[26] J. J. MacFarlane, I. E. Golovkin, P. Wang, P. R. Woodruff, and N. A. Pereyra, High Energy Density Phys. **3**, 181 (2007).

[27] A. S. Martynenko, I. Y. Skobelev, and S. A. Pikuz, Appl. Phys. B **125**, 31 (2019).